Design and characterization of optical-THz phase-matched traveling-wave photomixers

Shuji Matsuura* [a], Geoffrey A. Blake[a], Rolf A. Wyss[b], J. C. Pearson[b], Christoph Kadow[c], Andrew W. Jackson[c], and Arthur C. Gossard[c]

[a]Div. of Geological and Planetary Sciences, California Institute of Technology, Pasadena, CA 91125

[b]Jet Propulsion Laboratory, California Institute of Technology, Pasadena, CA 91109

[c]Materials Department, University of California, Santa Barbara, CA 93106

ABSTRACT

Design and characterization of optical-THz phase-matched traveling-wave photomixers for difference-frequency generation of THz waves are presented. A dc-biased coplanar stripline fabricated on low-temperature-grown GaAs is illuminated by two non-collinear laser beams which generate moving interference fringes that are accompanied by THz waves. By tuning the offset angle between the two laser beams, the velocity of the interference fringe can be matched to the phase velocity of the THz wave in the coplanar stripline. The generated THz waves are radiated into free space by the antenna at the termination of the stripline. Enhancement of the output power was clearly observed when the phase-matching condition was satisfied. The output power spectrum has a 3-dB bandwidth of 2 THz and rolls off as ~9 dB/Oct which is determined by the frequency dependent attenuation in the stripline, while the bandwidth of conventional photomixer design has the limitation by the RC time constant due to the electrode capacitance. The device can handle the laser power of over 380 mW, which is 5 times higher than the maximum power handring capability of conventional small area devices. The results show that the traveling-wave photomixers have the potential to surpass small area designs, especially at higher frequencies over 1 THz, owing to their great thermal dissipation capability and capacitance-free wide bandwidth.

Keywords: terahertz, LTG-GaAs, laser, photomixer, traveling-wave, phase-matching

1. INTRODUCTION

The difference frequency generation by optical-heterodyne mixing (photomixing) in low-temperature-grown (LTG) GaAs photomixers has been recently developed as a highly tunable solid-state source in the THz region.[1,2] In particular, diode-laser-based system has many advantages of wide tunability, compactness, low cost, high efficiency and easiness to handle.[3] It has already been proven that the photomixer is feasible as a light source for molecular spectroscopy,[4,5] and it would be suitable for the local oscillator of THz heterodyne receivers for astronomy and future telecommunication, especially for satellite-based instruments which demands compactness and tunability.

In most cases the spectral purity of the photomixer output is limited by the performance of the pump laser sources, and sufficiently high spectral performance for spectroscopic applications has now been achieved.[5,6] However, the output power is device-limited and insufficient for many applications until now. According to a simple photomixer theory,[1] the output power is proportional to the square of the photocurrent, which is proportional to both the pump laser power and the photoconductance. For conventional photomixers with a small active area, the bandwidth is limited by the carrier lifetime and the RC time constant due to the electrode capacitance coupled to the antenna impedance.[1] Since both the photoconductance and the capacitance are inversely proportional to the electrode gap width, photomixers have been designed to have small active areas ($\leq 10^2$ μm^2). However, such designs have limited power handling capabilities,[7] thus restricting the THz output power. The thermal damage threshold of typical LTG-GaAs film is <2 mW/μm^2, and the maximum laser power has been limited to ≤100 mW.

Similar output power limitation occures in high-speed photodetectors for microwave signal processing due to their low saturation intensity. In order to overcome this limitation, large area photodetectors operating in the traveling-wave mode have been proposed. The traveling-wave photodetector has advantages not only of high saturation intensity but also a

* Correspondence: Email: matsuura@gps.caltech.edu; Telephone: 626 395 3377; Fax: 626 585 1917

present address: Institute of Space and Astronautical Sciences, 3-1-1 Yoshinodai, Sagamihara, Kanagawa 229-8510, Japan

Part of the SPIE Conference on Terahertz and Gigahertz Photonics • Denver, Colorado • July 1999
SPIE Vol. 3795 • 0277-786X/99/$10.00

capacitance-free bandwidth, and this is true for the photomixer for the THz-wave generation as well. For traveling-wave photodetectors, it is necessary to match the velocity of the photo-induced carrier density wave and the phase velocity of the microwave signal, and various velocity (phase) matched devices have been developed. For an edge-illuminated optical waveguide traveling-wave photodetector, the phase-matching have been achieved by slowing down the microwave velocity with periodic loading of the microwave waveguide.[8] The 3-dB bandwidth of ~560 GHz has been demonstrated by utilizing an LTG-GaAs waveguide traveling-wave photodiode.[9] These optical waveguide traveling-wave photodetector designs would be applicable to the THz photomixer by scaling down the dimension and substituting two single-frequency lasers for the modulated single laser.[10] A vertically-illuminated device can also be operated in the traveling-wave mode; moving optical interference fringes induced by noncollinear multiple laser beams can be phase-matched to the microwave by tuning the incident angle. Moving optical interference fringes or photo-induced dynamic gratings have been commonly used in nonlinear optics related to photorefractive effects, four-wave mixing, ultra-fast carrier dynamics in semiconductors, etc.[11] As extension of these works, optoelectronic devices based on carrier density waves in semiconductor induced by the moving fringes have been proposed and demonstrated in the microwave regime.[12-16] The free space traveling-wave photomixer for the THz-wave generation has been first realized in our recent work.[17]

The traveling-wave photomixer that we proposed consists of a dc-biased coplanar stripline with a planar antenna fabricated on an LTG-GaAs photoconductive film. A large extent between the two metal striplines (~10^3 μm^2) is illuminated by noncollinear two laser beams that form traveling optical interference fringes on the device surface. The velocity of the optical fringes are matched to the phase velocity of THz waves in the stripline by varying the offset angle between the noncollinear laser beams. In our previous paper we described the device principle and demonstration of the THz-wave generation using a device with dipole antenna.[17] Since then, the antenna has been replaced to a log-periodic antenna in order to investigate the spectral property of the THz output and the internal efficiency in details eliminating the frequency dependence of the antenna. In this paper, we review the device principle and report recent measurement results. The stripline characteristics and its effect to the output power spectrum are discussed.

2. OPTICAL-THZ PHASE-MATCHING

As described above, the phase-matching for the free space traveling-wave photomixer is achieved by tuning the incident angle of the laser beams. In order to formulate the phase-matching condition, we consider a simple picture as shown in Fig. 1. When the photomixer surface is illuminated by two plane waves of frequency f_1 and f_2, and the wave vector of $\boldsymbol{k}_1$ and $\boldsymbol{k}_2$, respectively, the propagation constant of the interference fringe oscillating at the difference frequency, $f = f_1 - f_2$, ($\omega = 2\pi f = \omega_1 - \omega_2$, is given by the parallel (//) component of the difference of the two wave vectors, $\boldsymbol{k}_{op} = \boldsymbol{k}_1 - \boldsymbol{k}_2$. Since absorption occurs in a thin surface layer of ~1 μm, the photocarrier density have the same spatial distribution as the optical interference fringes on the surface. The velocity of the interference fringes along the surface is given by

$$v_{op} = \frac{\omega}{k_{op}^{//}} . \tag{1}$$

It is clear that the velocity can be tuned by changing the incident angles of the optical beams. The velocity of the THz wave in the stripline is

$$v_{THz} = \frac{c}{\sqrt{\varepsilon_{eff}}} , \tag{2}$$

where ε_{eff} is the effective dielectric constant and depends on the stripline geometry and the substrate thickness.[18] In the quasi static case that the stripline has no frequency dispersion, the effective dielectric constant can be defined as

$$\varepsilon_{eff} = \frac{\varepsilon_r + 1}{2} , \tag{3}$$

where ε_r is the dielectric constant of the substrate material (ε_r = 12.8 for GaAs). The phase-matching condition is satisfied when $v_{op} = v_{THz}$. This kind of angle-tuned phase-matching technique is the common technique for nonlinear three-wave mixing such as sum- and difference-frequency generation and optical parametric oscillator, and this is the limiting case that the interaction region is regarded as to be two-dimensional due to strong optical absorption in the material.

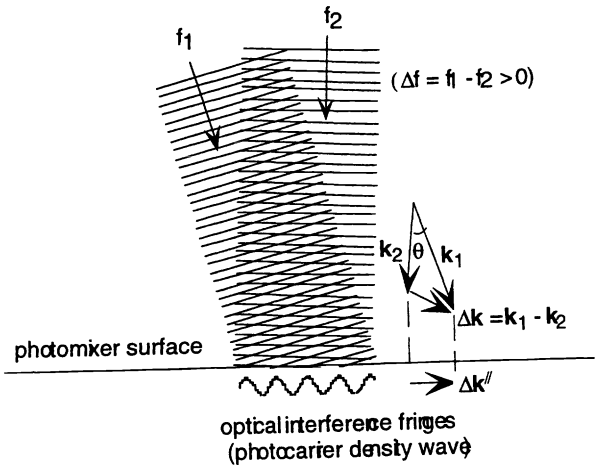

Fig. 1: The angle-tuned phase-matching scheme.

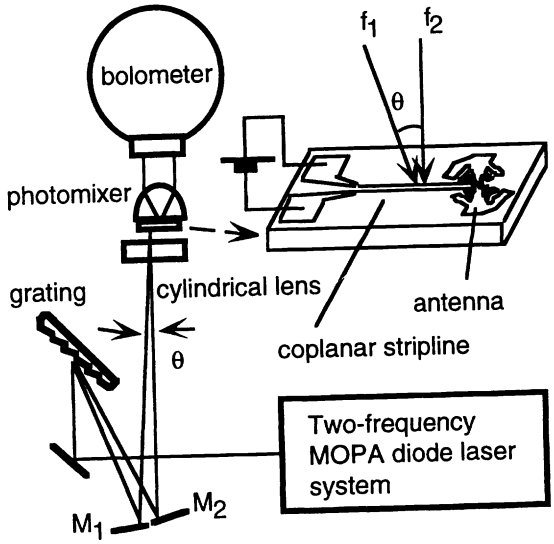

Fig. 2: Experimental setup.

3. EXPERIMENTAL SETUP

The photomixer used in the present experiment is a 1-μm thick LTG-GaAs film grown on semi-insulating GaAs substrates at 225° C and annealed for 30 s at 600° C. The photocarrier lifetime of the material measured by time resolved reflectance was 0.28 ps. Schematic view of the device is shown in the right upper of Fig. 2. The Ti/Pt/Au metal electrodes (0.02/0.02/0.2 μm thickness) fabricated on the LTG-GaAs consist of a 2-μm gap and 4-μm wide coplanar stripline. For this stripline geometry, the quasi static approximation (Eq. 3) is valid and the velocity dispersion should be less than 1% at the frequency below 3 THz.[18] One side of the stripline is terminated by a self-complimentary log-periodic antenna, and the other side is terminated by wire bonding pads for the dc bias, which has a tapered shape to reduce the reflection. The impedance of the log-periodic antenna of 72 Ω is well-matched to the stripline impedance of 76Ω, and the reflection by the mismatch should be negligible. Most of the THz output power from the antenna goes into the substrate because of its high dielectric constant, and the radiation is emitted to the free space through a hyper-hemispherical high-resistivity silicon lens attached to the back side of the substrate.

The experimental setup is shown in Fig. 2. The optical source is a two-frequency master oscillator power amplifier (MOPA) 850 nm semiconductor laser system.[19] A tapered semiconductor optical amplifier is simultaneously injection-seeded by a tunable external cavity laser (λ_1 = 848-853 nm) and a cavity-locked fixed frequency laser (λ_2 = 854 nm), and provides a maximum two-frequency power of 500 mW. The output from the MOPA is split into two beams by a 2000-groove/mm diffraction grating. Although it's not essential to use the grating for the phase-matching, and two individual laser sources can be used for the same experiment, the split collinear beam has the advantage of nearly identical spatial mode quality of the two colors, which is important to provide a well-ordered optical fringe pattern.

For a grating incidence angle of $\alpha = 50°$, the 1st order diffraction angle and its dispersion is $\beta = 70°$ and $d\beta/df = 0.8°$ THz^{-1}, respectively, and the diffraction efficiency was about 80%. The diffracted beams are reflected by two plane mirrors, and the mirror angle is adjusted to overlap the two laser beams on the photomixer surface. In the present experiment, the wave vector of the fixed frequency laser beam, k_2, is set to be perpendicular to the photomixer surface. For the GaAs substrate, the phase-matching condition is fulfilled when the offset angle between the two laser beams, θ, is approximately half the dispersion angle of the two beams, or $\theta \cong 0.5\Delta\beta$. The 3-mm diameter circular beam from the MOPA is converged to a ~200 μm × 2 μm FWHM beam at the photomixer surface with the combination of cylindrical lenses, and long direction of the beam is set to be parallel to the stripline. The maximum available laser power at the photomixer is about 380 mW.

The THz output power was measured with a silicon composite bolometer placed right in front of the photomixer to minimize the atmospheric absorption. Thermal emission caused by the laser and electrical power was estimated by operating the MOPA at a single frequency but the same power as the two-frequency operation.

4. RESULTS AND DISCUSSIONS

4.1. Phase-matching

According to the device principle, the THz output power should be highly dependent on the phase mismatch. We consider the θ dependence of the THz output power. To simplify the analysis, we assume that the laser power density is uniform over the illuminated area with the length of L, and that the photocarrier density wave is not affected by the interaction with the generated THz wave such as the parametric interaction. The forward ac current wave, which propagates to the same direction as the interference fringe, generated by the carrier density wave in a small unit length of the stripline at a position x and observed at the edge of the active area (L), is expressed as,

$$i(x) = i_0 e^{j(\omega t - k_{THz} L)} e^{j(k_{THz} - k_{op})x} , \tag{4}$$

where k_{THz} is the propagation constant of the THz wave, the active area is defined by $x = 0$ - L, and the initial phase of the carrier density wave at $t = 0$ and $x = 0$ is set to zero. Integrating the local contributions over the active area, the total current observed at x is given by,

$$I(L) = \int_0^L i(x)dx = i_0 e^{j(\omega t - k_{THz} L)} \frac{e^{j\Delta kL} - 1}{j\Delta k} , \tag{5}$$

where Δk is the phase mismatch,

$$\Delta k = k_{THz} - k_{op} = \omega\left(\frac{1}{v_{THz}} - \frac{1}{v_{op}}\right). \tag{6}$$

The THz power radiated from the antenna is then given by a well-known form,

$$P_{THz} = \frac{|I|^2 Z}{2} = \frac{I_0^2 Z}{2} \cdot \frac{\sin^2(\Delta kL/2)}{(\Delta kL/2)^2} , \tag{7}$$

where I_0 is the total ac current across the active area, $I_0 = i_0 L$, and Z is the antenna impedance. For the backward wave, the same expression as Eq. 7 with $\Delta k = k_{opt} + k_{THz}$ is derived. The backward wave decreases rapidly as the frequency increases, and its power level is less than 1% of the forward wave under the phase-matching condition for $f > 1$ THz and $L > 200$ μm. Therefore, the backward wave reflected back from the edge of the stripline should not interfere with the forward wave.

In the present experiment, the wave vector of the fixed frequency laser beam, k_2, is perpendicular to the photomixer surface, and the velocity of the optical fringes is expressed as,

$$v_{op} = \frac{c}{(1 + \omega_2 / \omega)\sin\theta} . \tag{8}$$

Fig. 3 presents the output power at 1 THz measured at various incident angles, namely the phase-mismatch curve. The data show a clear peak at $\theta = 0.43°$, which satisfies the phase-matching condition, as is expected from Eq. 2, 3 and 8. The calculated profile for $L = 280$ μm shows good agreement with the data and is consistent with the measured beam size of about 250 μm FWHM.

According to Eq. 8, for small θ and for $\omega_2 / \omega \gg 1$, the phase mismatch curve is independent on the THz-wave frequency, and the angle for the phase-matching has a linear dependence on the frequency. In fact, the profile measured at various frequencies were nearly identical to each other, and the angle for the phase-matching is nearly proportional to the frequency as shown in Fig. 4. The solid curve in Fig. 4 is the calculation from Eq. 2, 3 and 8 neglecting the dispersion of the

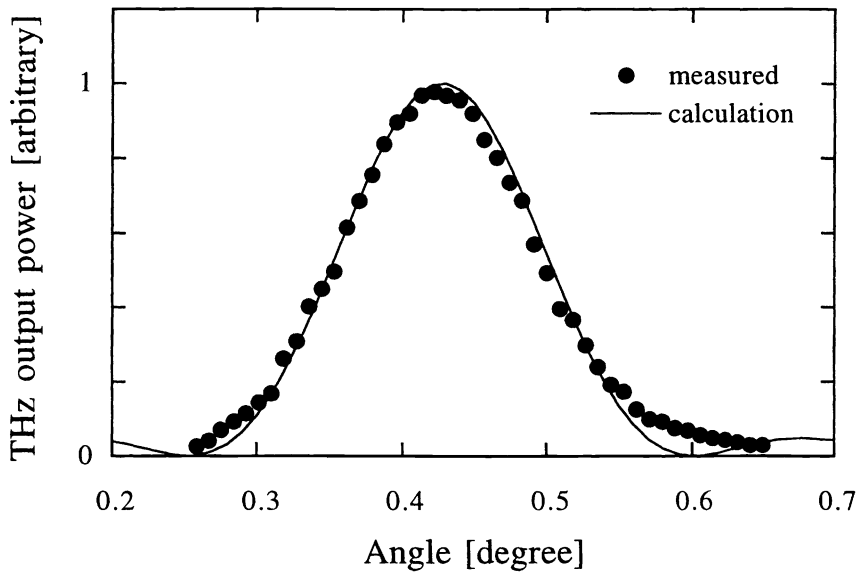

Fig. 3: The phase mismatch curve at f = 1 THz. The solid curve is the calculation from Eq. 7 with L = 250 μm.

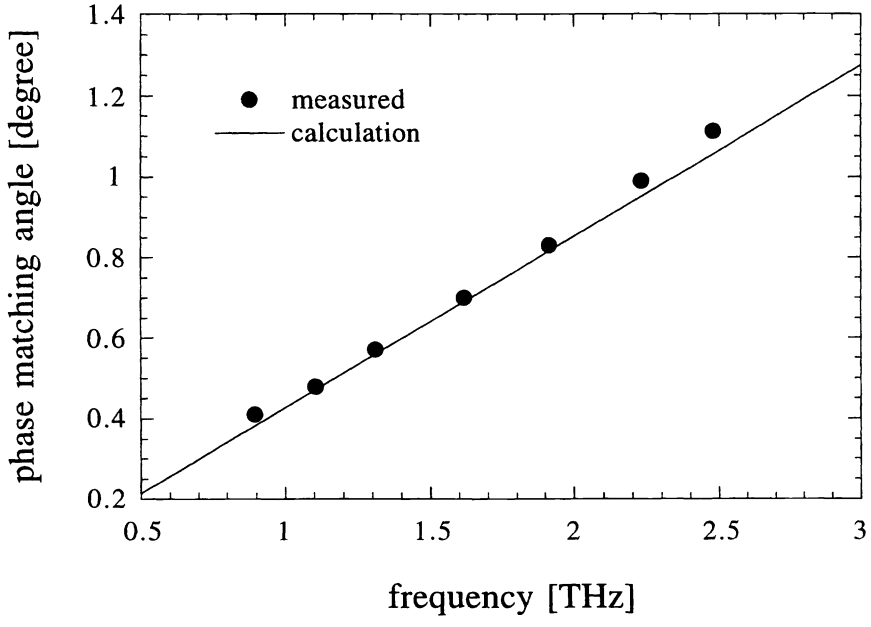

Fig. 4: The phase-matching angle vs the THz-wave frequency. The solid line is calculated from Eq. 2, 3 and 8.

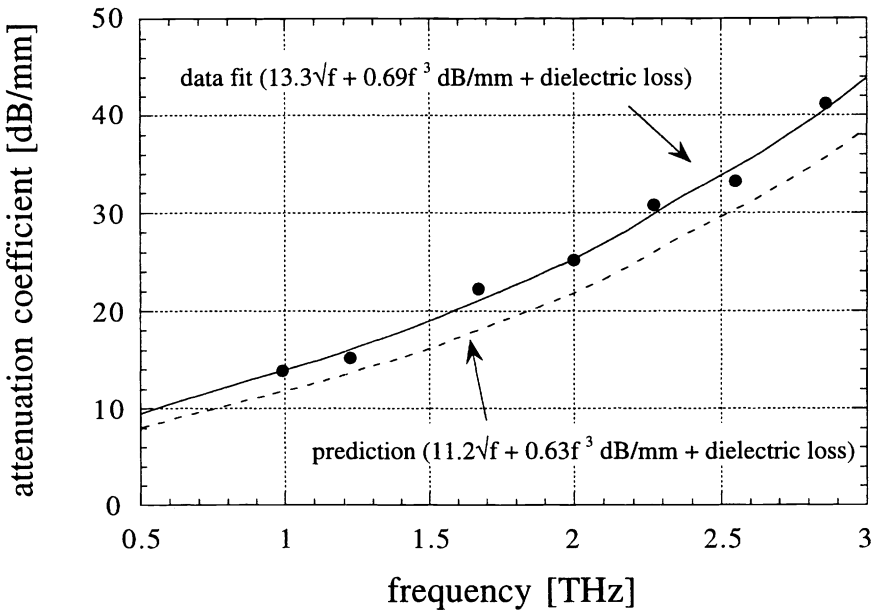

Fig. 5: The frequency dependent attenuation coefficient of the stripline. The solid curve is the result of data fitting with the form of Eq. 9, and the dashed curve is the prediction from Eq. 9. Both calculations are done with the dielectric loss estimated from the FTIR transmission measurement for the substrate.

substrate material and the stripline. The small scatter (≤5%) of the data from the calculation might be due to the dispersion of the stripline, while the total dispersion is estimated to be less than 2% at the frequency below 3 THz. The result shown in Fig. 3 and 4 give a proof that the present photomixer works as a phase-matched traveling-wave device.

4.2. Attenuation

The electromagnetic wave in a stripline on a thick dielectric substrate diminishes during the propagation due to conductor (ohmic) loss, dielectric loss, and radiation loss.[18,20,21] These losses have different frequency dependence, and the stripline geometry determine the dominant loss mechanism in the total attenuation. According to the frequency dependence of each loss, the total attenuation can be expressed as,

$$\alpha_{total} = \alpha_c \sqrt{f} + \alpha_r f^3 + \alpha_d f, \tag{9}$$

where α_c, α_r and α_d are attenuation coefficients for conductor loss, radiation loss and dielectric loss, respectively. The conductor loss calculated from the skin-effect resistance of the stripline gold metal is estimated to be α_c = 11.2 dB/mm/√THz. The radiation loss is due to the shock-wave radiation arising from the fact that the wave in the stripline propagates faster than in the substrate. The shock-wave radiation goes into the substrate with a cone angle determined by the velocity difference. The attenuation due to the radiation loss is expected to be α_r = 0.63 dB/mm/THz^3. The dielectric loss arises from the free carrier absorption and the phonon bands absorption of the substrate material, and its frequency dependence is complicated. In order to derive the attenuation coefficient by the dielectric loss, we measured the transmittance of the GaAs substrate material with a FTIR spectrometer. The attenuation increases monotonically with increasing the frequency in a range below 3 THz, and the attenuation coefficient at 3 THz is estimated to be α_d = 0.70 dB/mm/THz.

We measured the attenuation in the photomixer by measuring the THz output power with varying the laser spot position along the stripline. Fig. 5 presents the measured attenuation coefficient at various frequencies. The solid curve in the figure is the result of data fitting with the expression of Eq. 9 by fixing the dielectric loss coefficient to the predicted value. The attenuation coefficients obtained by the data fit is similar to but slightly higher than the predicted value as is indicated

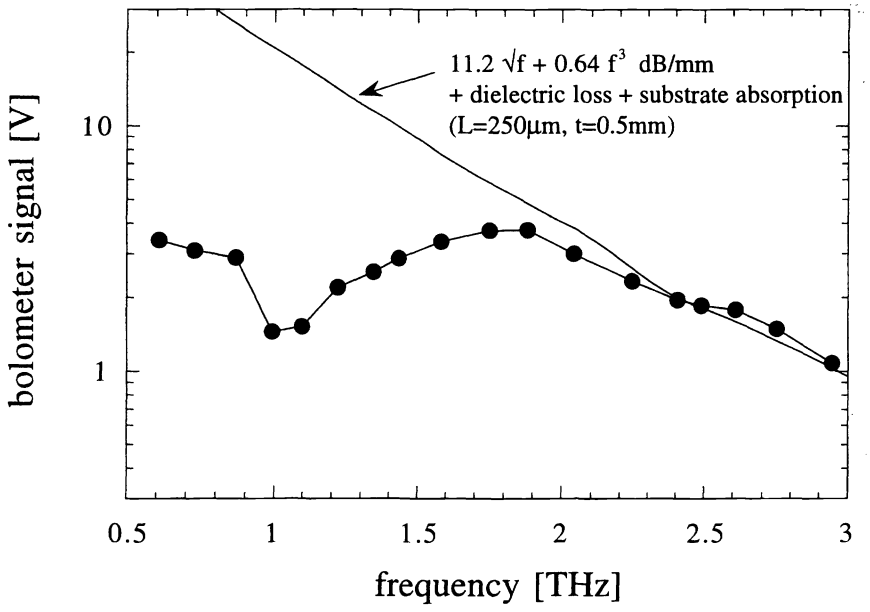

Fig. 6: The frequency dependence of the THz output power. The solid curve indicates the predicted frequency dependence by taking into account the stripline losses, the substrate absorption, and the carrier lifetime.

by the dashed curve. This discrepancy might be due to the ohmic loss enhancement arising from the localization of the ac electric field to a small area near the electrode anode and due to the decrease of the metal conductivity arising from the temperature rise of the active area by the optical and ohmic heating.

4.3. Output power

Fig. 6 presents the observed bolometer signal for the THz output at various frequencies. The data show a very flat spectrum, and the 3-dB bandwidth of 2 THz is far beyond the carrier-lifetime-limited bandwidth of 600 GHz. The high frequency roll-off as 9 dB/Oct is seen at frequencies above 2 THz in contrast to the 12-dB/Oct roll-off and the 3-dB bandwidth of <1 THz for small area photomixer designs.[1] Owing to very wide bandwidth, the present device could provide substantial amount of the output power at higher frequencies above 2 THz which have never been achieved with small area photomixers.

The frequency dependence of the output power of the traveling-wave photomixer is basically determined by the high-frequency roll-off due to finite carrier lifetime of the LTG-GaAs material and by the frequency dependent attenuation in the stripline. The THz wave propagating in the substrate material experiences additional attenuation due to the substrate absorption, and the frequency dependence of this attenuation is same as the dielectric loss in the stripline as is described in the last section. According to the FTIR transmission measurement, the absorption loss by the 0.5-mm thick GaAs substrate that we employed for the photomixer was 1.5 dB at 3 THz, and the absorption coefficient measured here is twice larger than that for the samples in previous works.[22] The absorption of the high-resistivity silicon lens is negligible in a range below 3 THz, while 30% of the power is lost by the reflection at the non-AR-coated lens/air interface.

The solid curve in Fig. 6 is the calculation of the output power spectrum for the 250-μm long stripline, for which the carrier lifetime and the losses described above are taken into account. The amplitude of the calculation is scaled to fit the data at the high frequency end. The high frequency roll-off behavior of the data at frequencies above 2 THz is similar to the calculation but slightly slower than the prediction. This slight improvement for the roll-off behavior could be caused by the fact that the signal was maximized by tuning the laser spot position in the stripline for a given frequency. At higher frequencies, the active area should be positioned as close as possible to the antenna in order to minimize the attenuation, even though it results in loosing the laser power coupled out the stripline region. At lower frequencies the measured spectrum is much flatter than the calculation and has a broad trough centered at 1 THz. In order to obtain the definite

interpretation for the measured spectrum, further theoretical consideration and measurements for various devices with different electrode structures are required.

According to the bolometer calibration with blackbody loads, the signals shown in Fig. 8 correspond to 0.05-0.2 μW. The predicted output power is ≥1 μW in the frequency range below 3 THz for the observed dc-photocurrent of 4 mA. At present, the cause of this large discrepancy between the measurement and the prediction is not clear. It might be due to shallow modulation depth of the optical interference fringes, or non-uniform bias fields in the active area which may cause the amplitude difference between the dc-photocurrent and the ac-photocurrent that contributes to generate the THz wave. Even though the measured power levels is the order of 0.1 μW, the traveling-wave photomixer described here would be useful for molecular spectroscopy, especially at frequencies above 2 THz where the small area photomixer has never been used for spectroscopy[5,23,24]

5. SUMMARY

We described basic characteristics of newly designed free space traveling-wave photomixers based on the angle-tuned phase-matching. The device has worked properly and showed the enhancement of the output power under the phase-matching condition. The 0.1-μW level output power with very flat spectrum extending over 3 THz, that is useful for spectroscopic applications, have been obtained. Large discrepancy between the measured the output power spectrum and the prediction from a photomixer theory. Further analysis and detailed modeling for the photomixer, including the consideration of the nonlinear interaction between the carrier density wave and the generated THz wave, may be required to fully understand the device characteristics.

There are several practical ways to increase the output power. Since the laser power density per unit area is presently ~1/5 of the thermal damage threshold, the increase of the laser power reflects directly the THz output power. The substrate absorption at higher frequencies can be decreased by employing the silicon substrate instead of GaAs. The radiation loss can be reduced by narrowing the total stripline width and employing a very thin substrate. The silicon based photomixer offers additional benefit of high power handling capability. A sandwiched endfire antenna structure with a superstrate would also eliminates the radiation loss. Since the conductivity of metal is strong function of the temperature, cooling the device should help to decrease the conductor loss in the stripline. By combining these factors, one order of magnitude output power improvement would be achieved.

ACKNOWLEDGMENT

The authors would like to thank T. E. Turner in the Microelectronics Device Laboratory at JPL for device fabrication. This research was sponsored by the Jet Propulsion Laboratory, California Institute of Technology, and the National Aeronautics and Space Administration. The work performed at UCSB was supported by the Center for Nonstoichiometric III-V Semiconductors.

REFERENCES

1. E. R. Brown, F. W. Smith, and K. A. McIntosh, *J. Appl. Phys.*, **73**, 1480 (1993).
2. E. R. Brown, K. A. McIntosh, F. W. Smith, K. B. Nichols, M. J. Manfra, C. L. Dennis, and J. P. Mattia, *Appl. Phys. Lett.*, **64**, 3311 (1994).
3. K. A. McIntosh, E. R. Brown, K. B. Nichols, O. B. McMahon, W. F. DiNatale, and T. M. Lyszczarz, *Appl. Phys. Lett.*, **67**, 3844 (1995).
4. S. Matsuura, M. Tani, and K. Sakai, *Appl. Phys. Lett.*, **70**, 559, (1997).
5. P. Chen, G. A. Blake, M. C. Gaidis, E. R. Brown, K. A. McIntosh, S. Y. Chou, M. I. Nathan, and F. Williamson, *Appl. Phys. Lett.* **71**, 1601 (1997).
6. S. Matsuura, P. Chen, G. A. Blake, J. C. Pearson, and H. M. Pickett, , *IEEE Trans. Microwave Theory and Tech.*, (1999), in press.
7. S. Verghese, K.A. McIntosh, and E.R. Brown, *IEEE Trans. Microwave Theory and Tech.*, **45**, 1301 (1997).
8. L. Y. Lin, M. C. Wu, T. Itoh, T. A. Vang, R. E. Muller, D. L. Sivco, and A. Y. Cho, *IEEE Phton. Technol. Lett.*, **8**, 1376 (1996).
9. Y. -J. Chiu, S. B. Fleischer, and J. E. Bowers, *IEEE Phton. Technol. Lett.*, **10**, 1021 (1998).

10. E. K. Duerr, K. A. McIntosh, and S. Verghese, *Proc. of the Tenth Int. Symp. on Space Terahertz Tech.* (1999), in press
11. H.J. Eichler, P. Günter, and D.W. Pohl, *Laser-Induced Dynamic Gratings,* (Springer-Verlag, Berlin, 1986).
12. A. Kostenbauder, S.J.B. Yoo, and A.E. Siegman, *IEEE J. of Quantum. Electron.*, **24**, 240, (1988).
13. H. Merkelo, B.D. McCredie, M.S. Veatch, A.G. Zocher, and T. Spanos, *IEEE J. of Quantum. Electron.*, **24**, 245, (1988).
14. U. Haken, M. Hundhausen, and L. Ley, *Appl. Phys. Lett.*, **63**, 3066, (1993).
15. D. Dolfi, Th. Merlet, A. Mestreau, and J.-P. Huignard, *Appl. Phys. Lett.*, **65**, 2931, (1994).
16. Th. Merlet, D. Dolfi, P. Collot, J. Nagle, and J.-P. Huignard, *Appl. Phys. Lett.*, **72**, 1134, (1998).
17. S. Matsuura, G. A. Blake, R. A. Wyss, J. C. Pearson, C. Kadow, A. W. Jackson, and A. C. Gossard, *Appl. Phys. Lett.*, **74**, 2872, (1999).
18. M.Y. Frankel, S. Gupta, J.A. Valdmanis, and G.A. Mourou, *IEEE Trans. Microwave Theory and Tech.*, **39**, 910 (1991).
19. S. Matsuura, P. Chen, G. A. Blake, J. C. Pearson, and H. M. Pickett, *Int. J. of Infrared and Millimeter Waves*, **19**, 849 (1998).
20. K. C. Gupta, R. Garg, and R. Chadha, *Computer-aided Design of Microwave Circuits*, (Artech House, Norwood, MA, 1981), p. 72.
21. D. B. Rutledge, D. P. Neikirk, and D. P. Kasilingam, in *Infrared and Millimeter Waves*, edited by K. J. Button (Academic Press, New York 1983), Vol. 10, p. 1.
22. C.J. Johnson, G.H. Sherman, and R. Weil, *Appl. Optics*, **8**, 1667 (1969).
23. A.S. Pine, R.D. Suenram, E.R. Brown, and K.A. McIntosh, J. Mol. Spec., **175**, 37 (1996).
24. S. Matsuura, M. Tani, H. Abe, K. Sakai, H. Ozeki, and S. Saito, J. Mol. Spec., **187**, 97 (1998).